

RESEARCH

Open Access



# Preoperative DBT-based radiomics for predicting axillary lymph node metastasis in breast cancer: a multi-center study

Shuyan He<sup>1,3</sup> , Biao Deng<sup>5,6</sup>, Jiaqi Chen<sup>4</sup>, Jiamin Li<sup>5</sup>, Xuefeng Wang<sup>6</sup>, Guanxing Li<sup>1,2</sup>, Siyu Long<sup>1,2</sup>, Jian Wan<sup>2</sup> and Yan Zhang<sup>1,2\*</sup>

## Abstract

**Background** In the prognosis of breast cancer, the status of axillary lymph nodes (ALN) is critically important. While traditional axillary lymph node dissection (ALND) provides comprehensive information, it is associated with high risks. Sentinel lymph node biopsy (SLND), as an alternative, is less invasive but still poses a risk of overtreatment. In recent years, digital breast tomosynthesis (DBT) technology has emerged as a new precise diagnostic tool for breast cancer, leveraging its high detection capability for lesions obscured by dense glandular tissue.

**Purpose** This multi-center study evaluates the feasibility of preoperative DBT-based radiomics, using tumor and peritumoral features, to predict ALN metastasis in breast cancer.

**Methods** We retrospectively collected DBT imaging data from 536 preoperative breast cancer patients across two centers. Specifically, 390 cases were from one Hospital, and 146 cases were from another Hospital. These data were assigned to internal training and external validation sets, respectively. We performed 3D region of interest (ROI) delineation on the cranio-caudal (CC) and mediolateral oblique (MLO) views of DBT images and extracted radiomic features. Using methods such as analysis of variance (ANOVA) and least absolute shrinkage and selection operator (LASSO), we selected radiomic features extracted from the tumor and its surrounding 3 mm, 5 mm, and 10 mm regions, and constructed a radiomic feature set. We then developed a combined model that includes the optimal radiomic features and clinical pathological factors. The performance of the combined model was evaluated using the area under the curve (AUC), and it was directly compared with the diagnostic results of radiologists.

**Results** The results showed that the AUC of the radiomic features from the surrounding regions of the tumor were generally lower than those from the tumor itself. Among them, the Signature<sub>tumor+10 mm</sub> model performed best, achieving an AUC of 0.806 using a logistic regression (LR) classifier to generate the RadScore. The nomogram incorporating both Ki67 and RadScore demonstrated a slightly higher AUC (0.813) compared to the Signature<sub>tumor+10 mm</sub> model alone (0.806). By integrating relevant clinical information, the nomogram enhances potential clinical utility. Moreover, it outperformed radiologists' assessments in predictive accuracy, highlighting its added value in clinical decision-making.

\*Correspondence:

Yan Zhang  
doctorzhangyan@vip.163.com

Full list of author information is available at the end of the article



© The Author(s) 2025. **Open Access** This article is licensed under a Creative Commons Attribution-NonCommercial-NoDerivatives 4.0 International License, which permits any non-commercial use, sharing, distribution and reproduction in any medium or format, as long as you give appropriate credit to the original author(s) and the source, provide a link to the Creative Commons licence, and indicate if you modified the licensed material. You do not have permission under this licence to share adapted material derived from this article or parts of it. The images or other third party material in this article are included in the article's Creative Commons licence, unless indicated otherwise in a credit line to the material. If material is not included in the article's Creative Commons licence and your intended use is not permitted by statutory regulation or exceeds the permitted use, you will need to obtain permission directly from the copyright holder. To view a copy of this licence, visit <http://creativecommons.org/licenses/by-nc-nd/4.0/>.

**Conclusions** Radiomics based on DBT imaging of the tumor and surrounding regions can provide a non-invasive auxiliary tool to guide treatment strategies for ALN metastasis in breast cancer.

**Clinical trial number** Not applicable.

**Keywords** DBT, Radiomics, Machine learning, Axillary lymph node

## Introduction

Axillary lymph node status is crucial in breast cancer diagnosis and prognosis, with direct implications for clinical decision-making and patient treatment outcomes [1, 2]. Traditionally, axillary lymph node dissection (ALND) has been considered the gold standard for assessing lymph node status [3]; however, this procedure is associated with significant complications, such as upper limb lymphedema, infection, and tumor dissemination. With the emergence of sentinel lymph node biopsy (SLND), lymph node evaluation has gradually shifted towards a more minimally invasive approach, but SLND may still result in overtreatment in some patients [4].

Digital breast tomosynthesis (DBT) is an advanced imaging technique that has revolutionized breast cancer screening and diagnosis by providing three-dimensional views of the breast. Studies have shown that DBT enhances the detection of breast lesions, particularly in dense breasts and overlapping structures [5].

Although DBT images are typically evaluated in detail by experienced radiologists, the interpretation process may still be somewhat subjective, and DBT exams do not fully cover all axillary lymph nodes, which limits the completeness of the assessment. To address this challenge, radiomics—the process of extracting high-dimensional, quantitative features from medical images—has been applied to breast imaging [6]. DBT radiomics enables the objective analysis of tumor characteristics and the surrounding environment, potentially improving the accuracy of ALN status prediction.

Previous studies have explored the applications of artificial intelligence (AI) in DBT, including deep learning, radiomics, and radiogenomics [7–9]. These studies have primarily focused on early breast cancer detection, the classification of benign and malignant lesions, molecular subtype evaluation, and the prediction of treatment response [10, 11].

From the perspective of tumor biology, the radiomics features of the intratumoral region, such as gray-level co-occurrence matrix entropy and wavelet transform texture, can quantitatively characterize the degree of intratumoral heterogeneity and cell proliferation activity [12], while the peritumoral region reflects the complex biological interaction process at the tumor-host interface, including the distribution of immune cells, angiogenesis status and interstitial structure [13]. A previous study demonstrated that a predictive model for axillary lymph

node (ALN) metastasis, constructed from radiomic features extracted from digital breast tomosynthesis (DBT) images, could significantly improve the accuracy of diagnostic imaging in breast cancer [14]. However, despite these significant advances, prior research on sentinel lymph node (SLN) status prediction has concentrated on the tumor region within the breast [15–17]. There is a relative lack of research on using radiomic features from both the tumor and peritumoral region, combined with clinical data, to comprehensively assess axillary lymph node (ALN) status. To fill this research gap, this study aims to explore and develop an innovative pre-operative assessment tool based on DBT technology, which analyzes radiomic features from both the tumor and surrounding regions and integrates patient clinical and pathological characteristics to predict axillary lymph node metastasis (ALNM) in early breast cancer patients.

## Method

### Patients

This retrospective multicenter analysis was approved by the institutional review boards of both centers and did not require informed consent. A total of 390 patients were recruited from Guangdong women and Children Hospital (from January 2021 to June 2023) and 146 patients from Guangdong Medical University Affiliated Hospital (from March 2019 to June 2023), all of whom had pathologically confirmed invasive breast cancer. The inclusion criteria were: (a) female patients with histologically confirmed invasive breast cancer; (b) patients with pathologically confirmed axillary lymph node (ALN) status; (c) patients who underwent preoperative digital breast tomosynthesis (DBT) imaging with lesions confirmed as masses or masses with calcification. The exclusion criteria were: (a) patients without pathological results; (b) patients lacking preoperative DBT images; (c) patients with other tumors in the past or present.

According to the 2013 St. Gallen Consensus Conference [18], breast cancer is classified into four molecular subtypes: luminal A, luminal B, HER2-positive, and triple-negative. According to the BI-RADS classification, grades 1–3 are generally considered benign, while grades 4 and above may be considered malignant [19]. Basic patient information is provided in Table 1.

P-value < 0.05: significant difference between training and validation set.

**Table 1** Patient profiles

	Primary cohort		P* value	External validation cohort		P value
	Positive ALN (n = 156)	Negative ALN (n = 234)		Positive ALN (n = 49)	Negative ALN (n = 97)	
<b>Age(yrs)</b>	51.31 ± 10.634	52.44 ± 10.596	0.302	49.09 ± 10.071	54.38 ± 9.573	0.003
<b>BI-RADS categories (%)</b>			0.000			0.129
3	6(3.8%)	14(6.4%)		0(0.0%)	2(2.1%)	
4a	9(5.8%)	9(4.1%)		4 (8.2%)	10(10.3%)	
4b	18(11.5%)	34(15.5%)		6(12.2%)	28(28.9%)	
4c	27(17.3%)	66(30.1%)		15(30.6%)	26(26.8%)	
5	96(61.5%)	96(43.8%)		24(49.0%)	31(32.0%)	
<b>Histological grade (%)</b>			0.433			0.802
/	33(21.2%)	53(22.6%)		6(12.2%)	14(14.4%)	
1	14(9.0%)	33(14.1%)		1(2.0%)	2(2.1%)	
2	78(50.0%)	107(45.2%)		14(28.6%)	32(33.0%)	
3	31(19.9%)	41(17.5%)		28(57.1%)	49(50.5%)	
<b>Estrogenic receptor (%)</b>			0.909			0.276
+	111(71.2%)	168(71.8%)		35(71.4%)	63(64.9%)	
-	45(28.8%)	66(28.2%)		14(28.6%)	34(35.1%)	
<b>Progesterone receptor (%)</b>			0.600			0.477
+	98(62.8%)	146(59.8%)		32(65.3%)	57(58.8%)	
-	58(37.2%)	98(40.2%)		17(34.7%)	40(41.2%)	
<b>HER-2 (%)</b>			0.738			0.220
+	50(32.1%)	71(30.3%)		28(57.1%)	44(45.4%)	
-	106(67.9%)	163(69.7%)		21(42.9%)	53(54.6%)	
<b>Ki-67 status (%)</b>			0.001			0.029
>20%	119(76.3%)	141(60.3%)		46(93.9%)	77(79.4%)	
≤ 20%	37(23.7%)	93(39.7%)		3(6.1%)	20(20.6%)	
<b>Molecular subtype (%)</b>			0.022			0.687
Luminal A	29(18.6%)	73(31.2%)		4(8.2%)	8(8.2%)	
Luminal B	89(57.1%)	101(43.2%)		28(57.1%)	57(58.8%)	
HER2 positive	19(12.2%)	29(12.4%)		14(28.6%)	21(21.6%)	
TNBC	19(12.2%)	31(13.2%)		3(6.1%)	11(11.3%)	

### Machine parameters

GE Senographe Essentia and Fuji AMULET Innovality digital breast tomography system were used in the image data set of our hospital. All patients were routinely photographed in the head and caudal position of the breast (eraniocaudal, CC) and mediolateral oblique (MLO), the acquisition mode was sector step-exposure scanning, automatic rotation acquisition: X-ray tube swing Angle was 25°(± 12.5°), 15°(± 7.5°); The acquisition time was < 10s. The imaging data were acquired using a digital breast tomography system (Hologic model: Hologic Selenia) with the following technical parameters in other hospitals: the imaging system used automatic exposure technology (Comb mode), and standardized projection position images were obtained in CC and MLO positions, respectively. Automatic rotation acquisition: X-ray tube swing Angle was 15°; The acquisition time was < 5s. All machine images were processed by 3D reconstruction algorithm to generate breast tomovolume images. All raw data and reconstructed results were archived in accordance with the DICOM standard.

### Segmentation and feature extraction

To ensure the reproducibility of the feature extraction process, all images were resampled and normalized to a uniform voxel spacing of 1 mm×1 mm×1 mm. The segmentation of the region of interest (ROI) was manually sketched by a radiologist with 5 years of experience who was unaware of the basic information and pathological findings of the images both positions CC and MLO were outlined along the edge of the lesion, outlining the lesion to show the clearest multi-layer images. For the mass with calcification, if the calcification was located inside the mass, the contour was delineated along the boundary of the mass. If the calcification was located around the mass, the suspected calcification was included in the ROI. Finally, all ROIs were reviewed by a senior radiologist with > 20 years of experience. In case of disagreement between the two radiologists, the lesion boundary was determined by the senior radiologist.

The segmentation and processing of ROIs were conducted on the Darwin Research Platform (<http://211.145.67.46:8590/> login), developed by Yizhun Medical AI Technology Co., Ltd. Based on relevant

literature on peritumoral analysis, tumor surrounding regions of 3 mm, 5 mm, and 10 mm were defined for analysis on the platform. The detailed workflow is illustrated in Fig. 1.

First, the ROI for the tumor mass was delineated and labeled as “Tumor.” The “Expand Mask” function was then used to generate 3 mm, 5 mm, and 10 mm

peritumoral region masks. This resulted in seven different models: (1) “Tumor” represents the tumor core region; (2) “Tumor + magin 3 mm” represents the tumor core plus a 3 mm surrounding peritumoral region; (3) “Tumor + magin 5 mm” represents the tumor core plus a 5 mm surrounding peritumoral region; (4) “Tumor + magin 10 mm” represents the tumor core plus

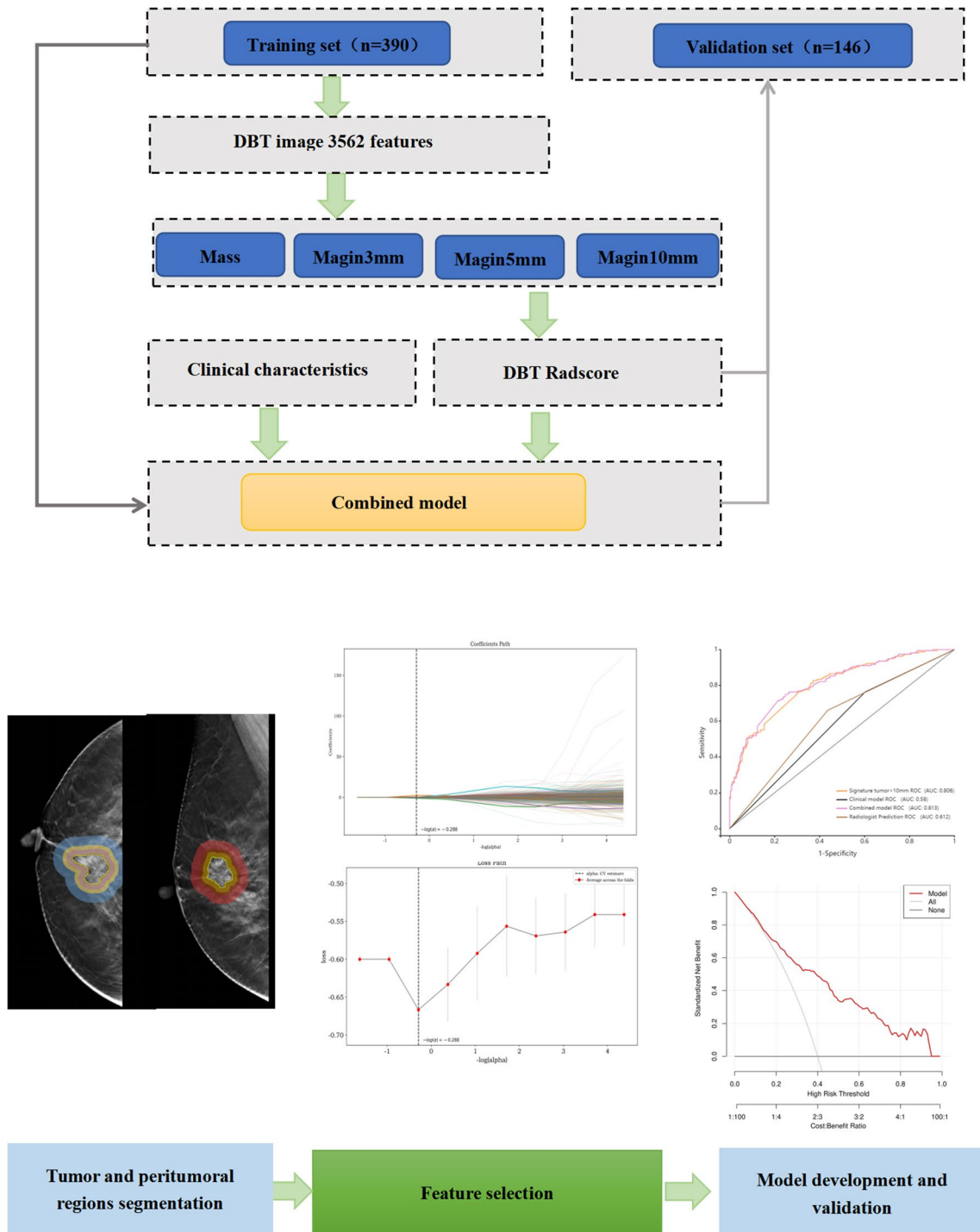


Fig. 1 The whole workflow in the study

a 10 mm surrounding peritumoral region; (5) “magin 3 mm” refers to the 3 mm surrounding peritumoral region only; (6) “magin 5 mm” refers to the 5 mm surrounding peritumoral region only; (7) “magin 10 mm” refers to the 10 mm surrounding peritumoral region only. All seven types of masks for each tumor mass were analyzed, and the images were grouped into seven sets to deeply analyze the characteristics of both the tumor core and surrounding areas.

Radiomic features were extracted using the Darwin research platform from the delineated intratumoral and peritumoral regions of interest (ROIs) on both cranio-caudal (CC) and mediolateral oblique (MLO) views. A total of 3 562 features were extracted from each intratumoral and 3 peritumoral ROIs, respectively, and 14 248 radiomics features were obtained for each patient. The extracted features encompassed several categories. Morphological features ( $n=28$ ) were derived from 3D geometrical parameters, including volume, surface area, compactness, flatness, maximum diameter, and sphericity deviation, which reflect spatial occupancy and morphological heterogeneity of the lesions. First-order statistical features ( $n=396$ ) quantified voxel intensity distribution within the ROIs, including metrics such as maximum, minimum, mean, median, skewness, kurtosis, and entropy, offering insights into enhancement heterogeneity and tissue-level changes like necrosis or calcification. Texture features were extracted to capture spatial relationships between voxels using gray level co-occurrence matrix (GLCM,  $n=528$ ), gray level run length matrix (GLRLM,  $n=352$ ), gray level size zone matrix (GLSZM,  $n=352$ ), gray level dependence matrix (GLDM,  $n=308$ ), and neighboring gray tone difference matrix (NGTDM,  $n=110$ ), thereby characterizing tumor micro-structural heterogeneity and spatial patterns. In addition, 1,488 wavelet features were derived using wavelet transform to capture multi-scale and localized image details, further enriching the radiomic representation of the tumor and its surrounding tissue.

### Model construction and validation

Patients from the two centers were divided into training and validation sets. To reduce overfitting and identify the most relevant features, we first performed feature selection using Analysis of Variance (ANOVA) and Least Absolute Shrinkage and Selection Operator (LASSO) algorithms on the training set. ANOVA was used to calculate the ratio of between-group variance to within-group variance (i.e., ANOVA-F value) for each feature using the `f_classif` function from the `sklearn` library, selecting features with a  $p$ -value less than 0.05. The best parameters (Alpha) for the LASSO algorithm were then determined to further select the relevant features. Finally, the Support Vector Machine Recursive Feature

Elimination (SVM-RFE) algorithm was applied for feature selection, identifying the minimal feature set that optimally predicted the model performance.

Based on the selected features, we constructed three machine learning models: Logistic Regression (LR), Support Vector Machine (SVM), and Extreme Gradient Boosting (XGBoost), and evaluated the models' robustness using 5-fold cross-validation. Previous studies have shown that these algorithms yield excellent performance in tasks such as tumor classification and lymph node metastasis prediction, supporting their applicability in this study context [20, 21].

Model performance was assessed by the Area Under the Receiver Operating Characteristic Curve (AUC-ROC), and additional metrics such as 95% confidence intervals (CI), sensitivity, and specificity were calculated.

After normalization, clinical variables were combined with the radiomic score (Radscore) using multivariate logistic regression analysis to establish a combined model. In addition to calculating the AUC, DeLong testing and calibration curves were performed. Finally, decision curve analysis (DCA) was used to assess the clinical utility of the combined model.

### Statistical analysis

All statistical analyses were performed using SPSS 26.0 and R software (version 4.0.3). The nomogram construction was performed using the “rms” package. For continuous variables, independent sample  $t$ -tests (for normal distribution) or Mann-Whitney  $U$  tests (for non-normal distribution) were used. For categorical variables, Fisher's exact test or chi-square tests were applied. The radiomics model was constructed using a multi-algorithm comparison strategy. Three Machine learning algorithms including LR, SVM and XGBoost were included. The clinical model, radiologist diagnostic model and Nomogram were all constructed based on the logistic regression framework. Statistical differences in the area under the receiver operating characteristic curve (AUC) were evaluated by DeLong test for performance comparison between models. In order to further evaluate the clinical application value of the clinical radiomics combined model, Decision Curve Analysis (DCA) was used to quantify the net benefits under different threshold probabilities. All statistical tests were two-sided, and the significance level was set at  $\alpha=0.05$ .

## Result

### Patient information

Table 1 summarizes the baseline characteristics, clinical, and pathological information of patients with breast masses in the internal and external validation groups. There were no statistically significant differences in histological grade, ER, PR and HER2 status between the two

sets ( $P > 0.05$ ). However, there were statistically significant differences in age, BI-RADS classification, Ki67 status, and molecular subtypes between the train or external validation set ( $P < 0.05$ ).

**Model construction and results**

Based on the DBT images of the tumor core and surrounding areas at 3 mm, 5 mm, and 10 mm, we extracted a total of 3,562 features from these images, followed by feature selection for each group. In order to ensure the scientificity and stability of feature selection, we used the three-step selection strategy of ANOVA, LASSO and SVM-RFE. Compared with the single selection method, this combination strategy not only removed redundant features and reduced the complexity of the model, but also retained the most predictive features to improve the robustness and generalization ability of the model. Using dimensionality reduction, 9 features were selected from the tumor region, and 9, 6, and 10 features were selected from the 3 mm, 5 mm, and 10 mm surrounding areas, respectively. The features from the tumor and

surrounding areas (3 mm, 5 mm, and 10 mm) were integrated to establish a radiomic model for the tumor core and surrounding regions, which quantitatively assesses the difference between patients with and without lymph node metastasis. The results of these models in both the train and validation sets are shown in Table 2. Among these models, the Signature<sub>tumor+10 mm</sub> model combining the Margin 10 mm region and the tumor demonstrated the highest diagnostic performance. Therefore, we selected this model to calculate the Radscore, which is given by the following formula:

$$\text{RadScore} = + 5.632 * \text{wavelet-HLH\_glcm\_Idn\_MLO\_MLO} + 5.490 * \text{logarithm\_firstorder\_Median\_CC\_CC-10 mm-3.890 * wavelet-LLH\_firstorder\_10Percentile\_CC\_CC-2.992 * log-sigma-3-0-mm-3D\_firstorder\_Skewness\_CC\_CC-2.759 * wavelet-HHL\_glszm\_LargeAreaLowGrayLevelEmphasis\_CC\_CC-10 mm} + 2.509 * \text{wavelet-LLL\_firstorder\_Kurtosis\_MLO\_MLO-2.435 * lbp-3D-k\_glszm\_SizeZoneNonUniformityNormalized\_MLO\_MLO-10 mm-2.266 * original\_glrlm\_ShortRunLowGrayLevelEmphasis\_MLO\_MLO-10 mm} + 2.209 * \text{expo}$$

**Table 2** Predictive performance of training and external validation sets

	Training set					External validation set				
	SEN	SPE	ACC	AUC	95%CI	SEN	SPE	ACC	AUC	95%CI
Mass										
LR	0.801	0.581	0.669	0.766	0.719–0.814	0.814	0.663	0.721	0.766	0.691–0.841
SVM	0.744	0.688	0.710	0.765	0.717–0.813	0.915	0.505	0.637	0.745	0.667–0.823
XGBOOST	0.756	0.675	0.708	0.789	0.744–0.834	0.745	0.626	0.664	0.712	0.625–0.798
Margin 3 mm										
LR	0.763	0.611	0.672	0.759	0.712–0.807	0.936	0.485	0.630	0.743	0.661–0.825
SVM	0.731	0.645	0.679	0.762	0.715–0.809	0.936	0.475	0.623	0.738	0.655–0.821
XGBOOST	0.801	0.585	0.672	0.755	0.707–0.803	0.745	0.606	0.903	0.651	0.617–0.799
Margin 5 mm										
LR	0.821	0.585	0.679	0.765	0.718–0.812	0.617	0.758	0.712	0.727	0.642–0.813
SVM	0.744	0.643	0.682	0.759	0.707–0.799	0.644	0.611	0.623	0.699	0.577–0.752
XGBOOST	0.950	0.552	0.706	0.756	0.791–0.869	0.797	0.526	0.630	0.695	0.577–0.751
Margin 10 mm										
LR	0.744	0.615	0.667	0.753	0.705–0.801	0.809	0.616	0.678	0.734	0.652–0.816
SVM	0.808	0.594	0.679	0.768	0.721–0.814	0.787	0.616	0.671	0.734	0.654–0.814
XGBOOST	0.776	0.577	0.656	0.749	0.700–0.797	0.745	0.646	0.646	0.696	0.602–0.790
Mass + Margin 3 mm										
LR	0.756	0.705	0.726	0.790	0.744–0.836	0.766	0.687	0.712	0.762	0.685–0.840
SVM	0.788	0.650	0.705	0.782	0.736–0.829	0.723	0.687	0.699	0.760	0.682–0.838
XGBOOST	0.853	0.594	0.697	0.799	0.756–0.843	0.660	0.697	0.685	0.697	0.607–0.788
Mass + Margin 5 mm										
LR	0.814	0.624	0.700	0.794	0.750–0.838	0.681	0.737	0.719	0.751	0.671–0.830
SVM	0.814	0.611	0.692	0.786	0.741–0.831	0.723	0.657	0.678	0.760	0.682–0.838
XGBOOST	0.872	0.594	0.705	0.800	0.757–0.843	0.638	0.768	0.726	0.728	0.642–0.813
Mass + Margin 10 mm										
LR	0.763	0.697	0.723	0.806	0.762–0.850	0.787	0.717	0.740	0.785	0.712–0.858
SVM	0.801	0.611	0.687	0.784	0.738–0.829	0.872	0.606	0.692	0.783	0.708–0.858
XGBOOST	0.808	0.637	0.705	0.798	0.754–0.843	0.830	0.646	0.705	0.772	0.697–0.846

SVM, support vector machine; LR, logistic regression; XGBOOST, eXtreme Gradient Boosting; AUC, area under the curve; SEN, sensitivity; SPE, specificity; ACC, accuracy

**Table 3** The results of multivariable logistic analysis in the training cohort

Characteristics	$\beta$	OR	95% CI	P value
BI-RADS categories(3;4a-5)	-0.268	0.765	0.282–2.077	0.599
Ki-67 status	-0.795	0.452	0.279–0.731	0.001
Age	0.004	1.004	0.984–1.024	0.696
Luminal/non-Luminal	-0.296	0.743	0.455–1.216	0.238

OR: Odds Ratio

$nential\_glszm\_SmallAreaHighGrayLevelEmphasis\_MLO\_MLO + 1.748 * wavelet-LHH\_ngtdm\_Coarseness\_MLO\_MLO - 10 \text{ mm} + 1.351 * \text{logarithm\_firstorder\_Root-MeanSquared\_CC\_CC} - 1.162 * \text{wavelet-HHL\_glcm\_Imc2\_MLO\_MLO} - 0.113.$

**Results of integrating radiomics and clinical models**

The Ki67 index was statistically different by multivariate logistic regression (Table 3) screening. The nomogram was constructed by combining the above clinically independent predictors and Radscore as shown in Fig. 2.

In the training set, the AUC (area under the curve) of the nomogram reached 0.813, demonstrating robust predictive performance.

Among the four models, the nomogram showed the best diagnostic efficiency in predicting lymph node

metastasis of breast cancer. Detailed comparative data are shown in Table 4. Figure 3A and B show the AUCs of the four models. Figure 3C and D show the decision curve analysis (DCA) results of each model of the nomogram in the training set and validation set, which further emphasizes the significant advantage of combining tumor and peritumoral features in improving the clinical predictive value. In addition, the calibration curves in Supplementary Fig. 1 show the agreement between the predicted probabilities of the nomogram model and the actual observed values in the training and validation sets.

**Discussion**

In this in-depth academic study, we systematically evaluated the intratumoral and peritumoral radiomic features derived from DBT images of BC patients, aiming to validate their effectiveness as preoperative predictors of ALN status and to propose an innovative predictive method. Specifically, we meticulously extracted 14,248 DBT radiomic features for each BC patient, and after rigorous dimensionality reduction, we constructed three advanced machine learning classifiers: SVM, LR, and XGBoost models. Results demonstrated that among all models, the Signature<sub>tuomor+10 mm</sub> model exhibited the most superior performance in both the training set and

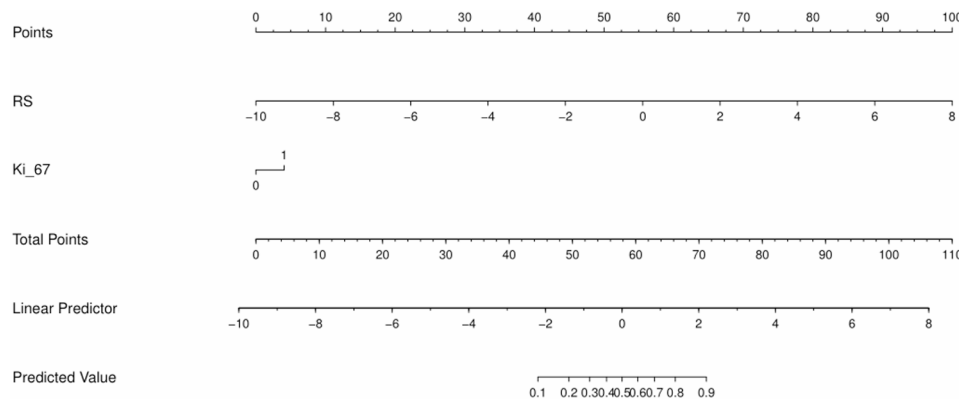


**Fig. 2** Nomogram

**Table 4** Performance of radiomics and clinical models in training and external validation cohort

DBT	AUC	Accuracy	SEN	SPE	PPV	NPV	P
<b>Training set</b>							
Signature <sub>tuomor+10 mm</sub>	0.806	0.723	0.763	0.697	0.626	0.815	<
Clinical model	0.580	0.544	0.763	0.397	0.458	0.715	<0.001
Nomogram	0.813	0.751	0.750	0.752	0.669	0.819	0.051
Radiologist	0.583	0.654	0.706	0.354	0.231	0.936	<0.001
<b>External validation set</b>							
Signature <sub>tuomor+10 mm</sub>	0.785	0.740	0.787	0.717	0.569	0.877	-
Clinical model	0.569	0.438	0.936	0.202	0.358	0.870	<0.001
Nomogram	0.792	0.726	0.851	0.667	0.548	0.904	0.184
Radiologist	0.582	0.705	0.611	0.719	0.234	0.929	<0.001

AUC: Area Under Curve, SEN: sensitivity, SPE: specificity, ACC: Accuracy, PPV: Positive Predictive Value, NPV: Negative Predictive Value. p values represent the delong test of the efficacy of each model compared with the Signature<sub>tuomor+10 mm</sub> model

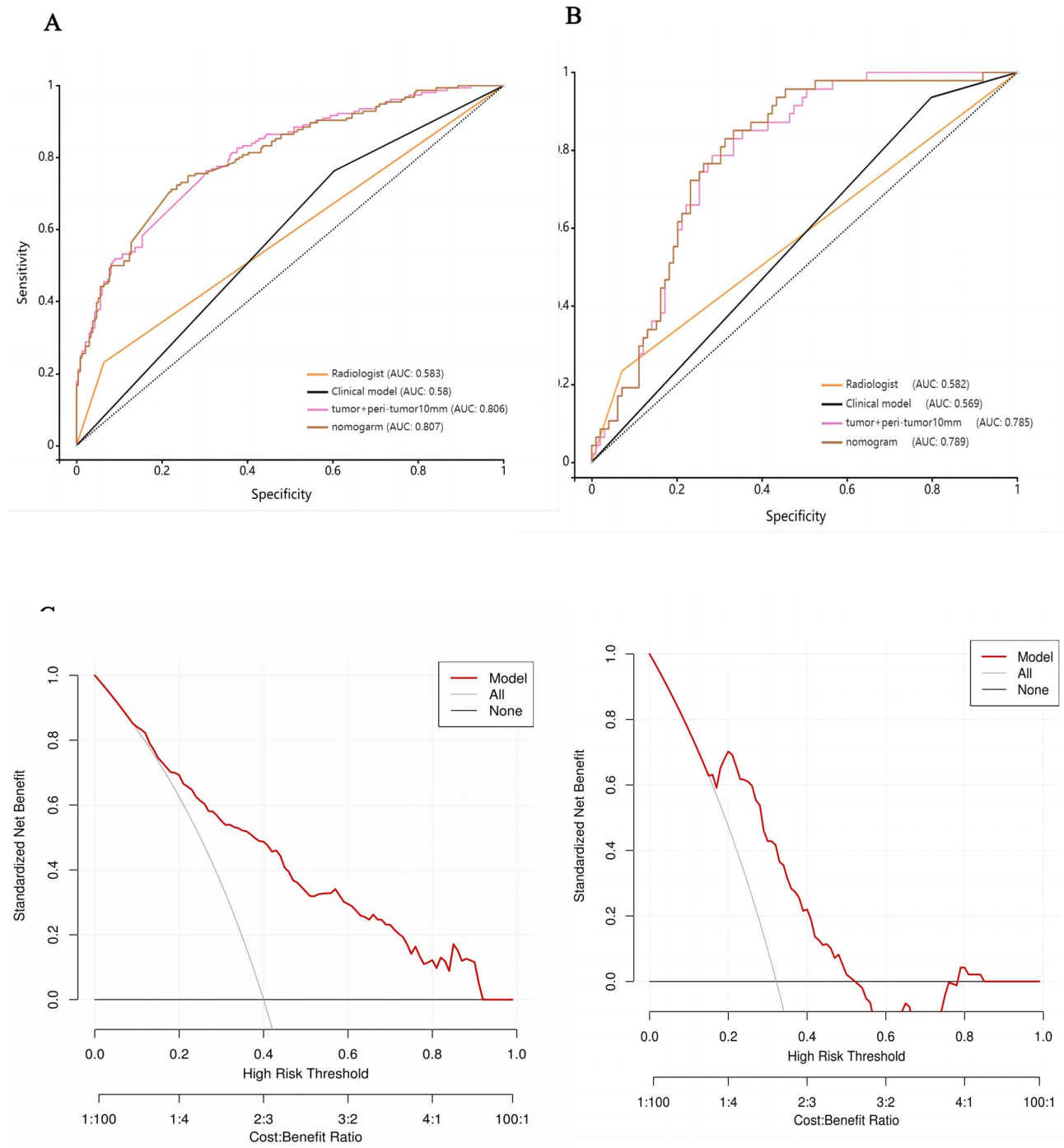


**Fig. 3** Figure A and B show the AUCs of the four models. Figures C and D present the decision curve analysis (DCA) of each model in the training and validation sets for the nomogram

external validation set, with area under the receiver operating characteristic (ROC) curve (AUC) values ranging from 0.784 to 0.806 and 0.772–0.785, respectively. The logistic regression (LR) model achieved the best performance, likely because the screened radiomic features exhibited a near-linear relationship with lymph node metastasis, allowing LR to better fit the data. This finding

aligns with previous studies using contrast-enhanced mammography (CEM) to analyze peritumoral features for predicting axillary lymph node metastasis [22], further supporting the critical role of intratumoral + peritumoral 10 mm radiomic features in evaluating nodal status. Feature importance analysis revealed that in the intratumoral model, the most predictive radiomic feature

was the wavelet feature `wavelet-HLH_glcm_Idn`, whereas in the 3 mm, 5 mm, and 10 mm peritumoral regions, the most significant features were all first-order features (`logarithm_firstorder_RootMean Squared`). This feature type was consistent with the findings of Cheng [23] et al.

The radiomic model incorporating the 10-mm peritumoral region demonstrated superior predictive performance compared to other peritumoral models, which may be attributed to a combination of biological and technical factors. Biologically, the peritumoral microenvironment within this range is known to be highly active in tumor–host interactions and is enriched with cancer-associated fibroblasts (CAFs), tumor-associated macrophages (TAMs), and infiltrating immune cells [24]. These components facilitate processes such as epithelial–mesenchymal transition (EMT), extracellular matrix remodeling, lymphangiogenesis, and lymphovascular invasion, all of which are critical for tumor metastasis [25, 26]. The 10-mm region may effectively capture these alterations, which are often missed in smaller peritumoral margins (e.g., 3–5 mm) due to limited spatial coverage. From a radiomics perspective, this region provides a balance between capturing sufficient biologically relevant information and maintaining signal stability without excessive interference from surrounding normal tissues, which may occur when larger margins are applied. Therefore, features extracted from this specific zone may more accurately reflect local stromal and immune alterations associated with axillary lymph node metastasis in breast cancer. This finding not only deepens our understanding of the biological behavior of breast cancer but also provides an important reference for preoperative planning in early BC patients, helping to reduce unnecessary surgical interventions and the risk of overtreatment [27].

Furthermore, this study conducted a comparative analysis between the intratumoral and peritumoral models and the peritumoral-only model, revealing that the model integrating both intratumoral and peritumoral information provided a more accurate depiction of the tumor. This finding is in line with the conclusions of Zhang et al. [28], which highlighted the limitations of relying solely on peripheral tissues for diagnosis, emphasizing the necessity of integrating both intratumoral and peritumoral information. AUC comparisons further validated this point, underscoring the superiority of the integrated model in predicting ALN status.

To more comprehensively assess the impact of Ki-67 expression levels on lymph node status, this study also employed multivariate logistic regression analysis, successfully identifying significant risk factors associated with high Ki-67 expression. Based on these findings, we developed a combined model incorporating Ki-67 and RadScore, aiming to further enhance prediction accuracy and reliability. The results indicated that the combined

model slightly outperformed the RadScore model alone in the validation set (AUC of 0.813 vs. 0.806), with similar high performance maintained in the training set (AUC of 0.792 vs. 0.785). This suggests that, while RadScore plays a dominant role in the model, Ki-67's risk factor provides additional value to the nomogram model for predicting lymph node status.

In the in-depth study exploring the correlation between Ki-67 expression levels and lymph node metastasis, we observed that cancer cells with high Ki-67 expression exhibited stronger proliferation and invasiveness, undoubtedly increasing their risk of metastasis via the lymphatic system. This observation aligns with previous research findings [29, 30], further reinforcing the role of Ki-67 as a critical biomarker for assessing tumor invasiveness and predicting lymph node metastasis potential. However, when attempting to combine Ki-67 with radiomics features to enhance predictive performance, we found that, despite a certain degree of performance improvement, the enhancement did not reach statistical significance. Similarly, in the study by Wu et al., despite integrating clinical features and radiomics information to predict Ki-67 status, no significant performance improvement was achieved. The common result of these two studies reveals an important fact: single or simple combined models have significant limitations in predicting complex biological phenomena.

However, the direct evaluation of digital breast tomosynthesis (DBT) images by radiologists for predicting lymph node metastasis has its limitations [31]. These limitations primarily stem from DBT's inability to comprehensively cover axillary lymph nodes. The complexity of lymph node metastasis involves multiple aspects, such as tumor cell invasion patterns, immune evasion mechanisms, and lymphatic invasion, making it difficult for visual interpretation alone to fully capture its dynamic changes and micro-characteristics [32, 33]. Additionally, subjective judgment differences among physicians, varying levels of experience, and factors such as visual fatigue may significantly affect diagnostic accuracy. This study also demonstrates that compared to traditional radiologist diagnostic models, radiomics models show statistically significant differences. In contrast, radiomics methods, driven by algorithms and automated extraction and analysis of numerous quantitative features, effectively reduce human biases, thereby enhancing prediction stability and objectivity. This approach not only captures lymph node metastasis-related features more comprehensively but also provides clinicians with more precise and reliable diagnostic support. In future work, prospective studies will be essential to further validate the robustness and generalizability of our model. Additionally, to facilitate clinical translation, strategies such as integrating the radiomics pipeline into radiology workstations

or PACS systems, and developing user-friendly software interfaces for real-time prediction, should be explored. These steps would enable clinicians to leverage radiomic insights in routine practice and potentially improve individualized decision-making for axillary lymph node management in breast cancer.

Regarding limitations, previous studies have indicated that incorporating hormone receptor status, such as ER and PR, can improve the performance of predictive models in breast cancer [22, 34]. However, in our study, no significant differences in these markers were found between the ALN metastasis and non-metastasis groups ( $p > 0.05$ ). This discrepancy may be due to the relatively small sample size ( $n = 536$ ) and heterogeneity in molecular subtype distribution. Further large-scale, multicenter prospective studies are needed to validate the predictive value of hormone receptor status in specific subtypes and its potential synergy with radiomic features. Although this study employed a dual-center design to enhance sample diversity and applied image resampling and normalization techniques to minimize inter-center variability, the overall sample size remained limited. Moreover, potential differences in imaging equipment between centers may still have introduced additional variability.

## Conclusion

This study, through a dual-center collaboration, proposes a combined model that integrates Ki-67 status and intratumoral and peritumoral radiomics features, demonstrating significant advantages in predicting axillary lymph node metastasis in breast cancer patients preoperatively. These findings provide a solid and reliable basis for developing personalized treatment strategies, although further validation and optimization are needed to enhance its application.

## Supplementary Information

The online version contains supplementary material available at <https://doi.org/10.1186/s12880-025-01711-3>.

Supplementary Material 1

## Acknowledgements

This work was supported by the Science and Technology Projects in Guangzhou (grant number: 202002030217).

## Author contributions

Guarantor of integrity of the entire study: ZY; study concepts and design: HSY, ZY; literature research: HSY, DB, CJQ; data collection: HSY, CJQ, WXF; data analysis: HSY, LGX, LSY, WJ; manuscript preparation: HSY, ZY, DB; manuscript review: LGX, LSY, WJ. All authors read and approved the final manuscript.

## Data availability

Data sets used and/or analyzed analysed during the current study are available from the corresponding authors upon reasonable request.

## Declarations

### Ethics approval and consent to participate

The study was conducted in accordance with the Declaration of Helsinki. This retrospective study was approved by the Ethics Committee of Guangdong women and Children Hospital and Guangdong Medical University Affiliated Hospital, and the requirements for written informed consent were waived.

### Consent for publication

Not applicable.

### Competing interests

The authors declare no competing interests.

### Author details

<sup>1</sup>Department of Radiology, Guangdong Women and Children Hospital, Guangzhou, China

<sup>2</sup>Women and Children's Hospital, Southern University of Science and Technology, Panyu District, Guangzhou, Guangdong Province, China

<sup>3</sup>Department of Radiology, The Second Affiliated Hospital of Guangzhou University of Chinese Medicine, Xiashan District, Guangzhou, Guangdong Province, China

<sup>4</sup>Department of Research & Development, Yizhun Medical AI Co. Ltd, Beijing, China

<sup>5</sup>Guangdong Medical University, Xiashan District, ZhanJiang, Guangdong Province, China

<sup>6</sup>Department of Cardiothoracic Surgery, Affiliated Hospital of Guangdong Medical University, ZhanJiang, China

Received: 21 January 2025 / Accepted: 5 May 2025

Published online: 19 May 2025

## References

- Zheng X, Yao Z, Huang Y, et al. Deep learning radiomics can predict axillary lymph node status in early-stage breast cancer [published correction appears in. *Nat Commun*. 2021;12(1):4370.
- Ghaffari A, Hoskin V, Turashvili G, et al. Intravital imaging reveals systemic Ezrin Inhibition impedes cancer cell migration and lymph node metastasis in breast cancer. *Breast Cancer Res*. 2019;21(1):12.
- Zheng S-Y, et al. The influence of axillary surgery and radiotherapeutic strategy on the risk of lymphedema and upper extremity dysfunction in early breast cancer patients. *Breast (Edinburgh Scotland)*. 2023;68:142–8.
- Giuliano AE et al. Axillary dissection vs no axillary dissection in women with invasive breast cancer and Sentinel node metastasis: a randomized clinical trial. *JAMA*. 2011;305(6):569–75.
- Chong A et al. Digital Breast Tomosynthesis: Concepts and Clinical Practice. *Radiology*. 2019;292(1):1–14.
- Conti A, et al. Radiomics in breast cancer classification and prediction. *Sem Cancer Biol*. 2021;72:238–50.
- Wang D, et al. Radiomics analysis on digital breast tomosynthesis: preoperative evaluation of lymphovascular invasion status in invasive breast Cancer. *Acad Radiol*. 2022;29(12):1773–82.
- Tagliafico AS, Bignotti B, Rossi F, et al. Breast cancer Ki-67 expression prediction by digital breast tomosynthesis radiomics features. *Eur Radiol Exp*. 2019;3(1):36.
- Xu L, Zhongzi X, Xuerui L, Ying C, Jing R, Peng Z. The relationship between three breast cancer molecular subtypes and digital breast tomosynthesis imaging features: based on bi-rads. *J Mol Imaging*. 2021;44(4):567–73.
- Jiang T, et al. Intratumoral analysis of digital breast tomosynthesis for predicting the Ki-67 level in breast cancer: A multi-center radiomics study. *Med Phys*. 2022;49(1):219–30.
- Hussain S, Lafarga-Osuna Y, Ali M, Naseem U, Ahmed M, Tamez-Peña JG. Deep learning, radiomics and radiogenomics applications in the digital breast tomosynthesis: a systematic review. *BMC Bioinformatics*. 2023;24(1):401.
- You C, Su GH, Zhang X, et al. Multicenter radio-multiomic analysis for predicting breast cancer outcome and unravelling imaging-biological connection. *NPJ Precis Oncol*. 2024;8(1):193.
- Wu PQ, Guo FL, Wang J, et al. Development and validation of a dynamic contrast-enhanced magnetic resonance imaging-based habitat and peritumoral radiomic model to predict axillary lymph node metastasis in

- patients with breast cancer: a retrospective study. *Quant Imaging Med Surg.* 2024;14(12):8211–26.
14. Haraguchi T, Goto Y, Furuya Y, et al. Use of machine learning with two-dimensional synthetic mammography for axillary lymph node metastasis prediction in breast cancer: a preliminary study. *Transl Cancer Res.* 2023;12(5):1232–40.
  15. Zha HL, Zong M, Liu XP, Pan JZ, Wang H, Gong HY, et al. Preoperative ultrasound-based radiomics score can improve the accuracy of the memorial sloan kettering cancer center nomogram for predicting Sentinel lymph node metastasis in breast cancer. *Eur J Radiol.* 2021;135:109512.
  16. Liu J, Sun D, Chen L, Fang Z, Song W, Guo D, et al. Radiomics analysis of dynamic contrast-enhanced magnetic resonance imaging for the prediction of Sentinel lymph node metastasis in breast cancer. *Front Oncol.* 2019;9:980.
  17. Shi W et al. Sep. Prediction of axillary lymph node metastasis using a magnetic resonance imaging radiomics model of invasive breast cancer primary tumor. *Cancer imaging: the official publication of the International Cancer Imaging Society.* Sep. 13 2024;24(1):122. <https://doi.org/10.1186/s40644-024-00771-y>
  18. Goldhirsch A, Winer EP, Coates AS, et al. Personalizing the treatment of women with early breast cancer: highlights of the St Gallen international expert consensus on the primary therapy of early breast Cancer 2013. *Ann Oncol.* 2013;24(9):2206–23.
  19. Lee KA, Talati N, Oudsema R, Steinberger S, Margolies LR. BI-RADS 3: current and future use of probably benign. *Curr Radiol Rep.* 2018;6(2):5.
  20. Lu G, Tian R, Yang W, et al. Deep learning radiomics based on multimodal imaging for distinguishing benign and malignant breast tumours. *Front Med (Lausanne).* 2024;11:1402967.
  21. Yan M, He D, Sun Y, et al. Comparative analysis of nomogram and machine learning models for predicting axillary lymph node metastasis in Early-Stage breast cancer: A study on clinically and Ultrasound-Negative axillary cases across two centers. *Ultrasound Med Biol.* 2025;51(3):463–74.
  22. Wang Z et al. Intra- and peritumoral radiomics of Contrast-Enhanced mammography predicts axillary lymph node metastasis in patients with breast cancer: A multicenter study. *Academic Radiology.* 2023;30(Suppl 2):S133–42.
  23. Cheng Y, Xu S, Wang H, et al. Intra- and peri-tumoral radiomics for predicting the Sentinel lymph node metastasis in breast cancer based on preoperative mammography and MRI. *Front Oncol.* 2022;12:1047572.
  24. Quail DF, Joyce JA. Microenvironmental regulation of tumor progression and metastasis. *Nat Med.* 2013;19(11):1423–37.
  25. Annaratone L, Cascardi E, Vissio E, Sarotto I, Chmielik E, Sapino A, et al. The multifaceted nature of tumor microenvironment in breast carcinomas. *Pathobiology.* 2020;87(2):125–42.
  26. Liang Y, Zhang H, Song X, Yang Q. Metastatic heterogeneity of breast cancer: molecular mechanism and potential therapeutic targets. *Semin Cancer Biol.* 2020;60:14–27.
  27. Krag DN, Anderson SJ, Julian TB, et al. Technical outcomes of sentinel-lymph-node resection and conventional axillary-lymph-node dissection in patients with clinically node-negative breast cancer: results from the NSABP B-32 randomised phase III trial. *Lancet Oncol.* 2007;8(10):881–8.
  28. Zhang W, et al. Ultrasound-based radiomics nomogram for predicting axillary lymph node metastasis in early-stage breast cancer. *La Radiologia Med Vol.* 2024;129(2):211–21.
  29. Jiang T, Song J, Wang X, Niu S, Zhao N, Dong Y, et al. Intratumoral and peritumoral analysis of mammography, tomosynthesis, and multiparametric MRI for predicting ki-67 level in breast cancer: a radiomics-based study. *Mol Imaging Biol.* 2022;24(4):550–9.
  30. Zhou D et al. Distribution characteristics and prognostic value of immune infiltration in oligometastatic breast cancer. *Front Oncol. Nov.* 2021;11:747012.
  31. Han L, Zhu Y, Liu Z, Yu T, He C, Jiang W, et al. Radiomic nomogram for prediction of axillary lymph node metastasis in breast cancer. *Eur Radiol.* 2019;29(7):3820–9.
  32. Xu M, et al. Radiomics nomogram based on digital breast tomosynthesis: pre-operative evaluation of axillary lymph node metastasis in breast carcinoma. *J cancer Res Clin Oncol.* 2023;149(11):9317–28.
  33. Blomberg OS, Kos K, Spagnuolo L, et al. Neoadjuvant immune checkpoint Blockade triggers persistent and systemic Treg activation which blunts therapeutic efficacy against metastatic spread of breast tumors. *Oncoimmunology.* 2023;12(1):2201147.
  34. Mao N, Bao Y, Dong C, et al. Delta radiomics based on MRI for predicting axillary lymph node pathologic complete response after neoadjuvant chemotherapy in breast Cancer patients. *Acad Radiol.* 2025;32(1):37–49.

## Publisher's note

Springer Nature remains neutral with regard to jurisdictional claims in published maps and institutional affiliations.